

Contents lists available at ScienceDirect

# Journal of Crystal Growth

journal homepage: www.elsevier.com/locate/jcrysgro



# Strain-balanced InGaAs/AlInAs/InP quantum cascade laser grown on GaAs by MOVPE

Shining Xu, Shuqi Zhang, Huilong Gao, Jeremy Kirch, Dan Botez, Luke Mawst

Department of Electrical and Computer Engineering, University of Wisconsin-Madison, 1415, Engineering Drive, Madison, WI 53706, USA

#### ARTICLE INFO

'Communicated by' Elke Meissner

Keywords:

A1. Substrates

A3. Metalorganic vapor phase epitaxy

A3. Laser epitaxy

A3. Superlattices

B2. Semiconductor III-V materials

B3. Quantum cascade lasers

#### ABSTRACT

A systematic study was performed to elucidate the properties of strained-layer InGaAs/AlInAs superlattices (SL) on metamorphic buffer layers grown by MOVPE on GaAs substrates. Differences observed in surface morphology indicate relatively tight control over the SL average net-strain is required for the growth of micron-thick SL structures, as needed for quantum cascade laser (QCL) active regions. Using such conditions, 5.7  $\mu$ m-emitting, strain-balanced InP-based QCLs grown on (001) GaAs were demonstrated with comparable device performance to their counterparts grown on native InP substrate. 3 mm-long and 25  $\mu$ m-wide uncoated-facets devices, grown on GaAs and having epi-side lateral contacts, provide peak-pulsed output powers of 2.65 W per facet at room temperature. The corresponding threshold-current density and maximum wall-plug efficiency is 1.61 kA/cm² and 6.0% respectively. HR-XRD measurements of the strain-balanced QCL grown on GaAs show broadened satellite peaks which are well aligned with the peaks from their counterparts grown on InP.

## 1. Introduction

Mid-infrared (IR) (i.e.,  $3-16 \mu m$ ) is an important wavelength range for applications ranging from chemical sensing to free-space optical communications. Over the past decade, strained-layer InGaAs/AlInAsbased quantum cascade lasers (QCLs) grown on InP substrates have achieved great advancements in the mid-IR spectral region by displaying low threshold-current densities and high output powers [1-3]. The development of InGaAs/AlInAs-based light sources grown on other substrate platforms, such as GaAs or Si, is desirable for reducing cost as well as for integration with mature electronic and photonic devices. Among all possible integration methods, integration via heterogeneous epitaxy is most attractive for silicon photonics involving massive chipscale fabrication. Mid-IR QCLs employing strained-layer InGaAs/AlInAs-based active regions on mismatched substrates such as GaAs or Si have been demonstrated but have been reported only when employing molecular beam epitaxy (MBE) growth [4-7]. To date, there are no reports of using metalorganic vapor phase epitaxy (MOVPE) method to realize such devices, while MOVPE is particularly suitable for industrial high-throughput and large-scale production of QCLs and is already widely established for other semiconductor lasers.

Previously, we have demonstrated the first InGaAs/AlInAs-based QCLs on GaAs substrate employing lattice-matched SL active regions (nominally zero individual layer strain) grown by MOVPE on metamorphic buffer layers (MBLs) for the long-wave mid-IR (8–16  $\mu m$ ) spectral region [8]. Those devices did show similar device performance compared to their counterparts grown on native InP substrate, thus

confirming earlier findings on long-MIR (8–12  $\mu$ m) wavelength QCLs, that performance metrics are relatively insensitive to high dislocation densities. In this work, we investigate the factors triggering crystal structural degradation of high-strain InGaAs/AlInAs superlattices (SLs) grown on an MBL, which had previously inhibited the growth of thick (micron-range thickness) strained SL active-regions, which are critical to realizing higher performance mid-IR QCLs.

We find that, although the InP buffer layer is up to 95–97% relaxed, the residual strain strongly affects the growth of 1  $\mu m$ -thick InGaAs/AlInAs SLs grown atop the MBL. SL surface morphology measurements using atomic force microscopy (AFM) and HR-XRD measurements, indicate that a small net-strain tolerance is present for QCL active regions formed without strain relaxation. Under appropriate growth conditions, a strain-balanced QCL on GaAs is demonstrated to display performance comparable to devices grown on native InP substrates.

### 2. Materials and methods

In this work, all materials, including the superlattices and the full laser structure, were grown at low pressure (100 torr) in a close-coupled showerhead (CCS) vertical MOVPE (3  $\times$  2 in. multi-wafer) reactor, using TMIn, TMAl, TMGa, AsH3, and PH3 as group III and group V precursors, diluted Si $_2$ H6 as the doping source, and H2 as the carrier gas at a temperature of 605 °C. The surface temperature is confirmed using in-situ pyrometry measurements. The InP buffer layer on (001) on-orientation GaAs used in this study was the same as that employed previously for realizing lattice-matched active- region QCLs on GaAs.

Low surface roughness, as low as 0.4 nm over  $10 \times 10 \text{ cm}^2$  area, and a threading-dislocation density around mid of  $10^8 \text{ cm}^{-2}$ , was reported for these buffer layers [8]. The value of the in-plane lattice constant for the InP buffer was estimated to be 0.5867 nm [8].

To examine the net strain effect and mimic the growth of the QCL active region, a 250-repetition SL structure composed of 2 nm  $\rm In_x Ga_{1-x} As$  and 2 nm  $\rm Al_y In_{1-y} As$  layers was chosen for reference. The fraction of indium (x) for the quantum wells and of aluminum (y) for the barriers was targeted at  $\sim 0.7$ , which is frequently employed for InP-based QCLs operating in the 4–6  $\mu$ m wavelength range. The SL net strain was calculated based on the thickness-weighted model without considering the elastic constant [9–11]:

$$\epsilon_{InGaAs} = \frac{(a_{sub} - a_{InGaAs}) \times t_{InGaAs}}{a_{sub}} \tag{1}$$

$$\epsilon_{AlGaAs} = \frac{(a_{sub} - a_{AlInAs}) \times t_{AlInAs}}{a_{res}} \tag{2}$$

$$\epsilon_{net} = \frac{\epsilon_{InGaAs} + \epsilon_{AIGaAs}}{t_{InGaAs} + t_{AIGaAs}} \tag{3}$$

where  $a_{sub}$  is the in-plane lattice constant of the InP buffer, which acts as the pseudo-morphic substrate, and the in-plane lattice constants for ternary wells ( $a_{InGaAs}$ ) and barrier layers ( $a_{AlInAs}$ ) are calculated using Vegard's law, with lattice constant values used for the relevant binary materials as,  $a_{GaAs} = 5.6533$  Å,  $a_{AlAs} = 5.6605$  Å,  $a_{InAs} = 6.0584$  Å, and  $a_{InP} = 5.8687$  Å. The strain of InGaAs layer is designated as  $\epsilon_{InGaAs}$  and strain of AlInAs layer is  $\epsilon_{AlInAs}$ , while the net strain of the SL is identified as  $\epsilon_{net}$ .

Since the designed thicknesses for InGaAs and AlInAs layers are identical, the calculation of the superlattice net strain can be simplified as such:

$$\epsilon_{net} = \frac{2a_{sub} - a_{InGaAs} - a_{AlInAs}}{2a_{sub}} \tag{4}$$

In the current study, the zero-stress method [12] was not utilized, which is an alternate strain-balancing approach that has been used in estimating the critical thickness. However, we find that the differences between zero-stress method and the thickness-weighted model are small for the strain values of interest in this study.

The individual layer composition/strain, V/III ratio, growth rate, and target net strain for the SL samples under study are shown in Table 1. Although the growth rates and V/III ratios utilized vary among samples, the differences are relatively small, thus it can be assumed that the growth conditions for all superlattice growths in this study are nominally the same.

The same growth conditions used for the superlattice study were then applied to the QCL growth, starting with a 200 nm-thick InP buffer, followed by a 300 nm-thick heavily doped  $(3\times10^{18}~\text{cm}^{-3})$   $In_{0.53}Ga_{0.47}As$  for lateral contact, and then the 2000 nm-thick lower-cladding InP layer  $(1\times10^{17}~\text{cm}^{-3})$ , followed by 300 nm-thick  $In_{0.53}Ga_{0.47}As$  (5  $\times$   $10^{16}~\text{cm}^{-3}$ ) light-confining layers on each side of the SL active region. The upper InP cladding layers consisted of 2000 nm-thick layer (n  $\sim$  2  $\times$   $10^{16}\text{cm}^{-3}$ ), a 1000 nm-thick (n  $\sim$  2  $\times$   $10^{17}\text{cm}^{-3}$ ) layer, and a 1000 nm-thick heavily doped (n  $\sim$  2  $\times$   $10^{19}\text{cm}^{-3}$ ) layer

serving as top contact layer. 2-inch, low-roughness InP-buffer-on GaAs [8] and another 2-inch native n-doped InP wafer were placed into the reactor at the same time as the laser growth, thus a direct comparison of device performance could be obtained.

A QCL based on a moderately-strained 30-stage active region,  $In_{0.60}Ga_{0.40}As/Al_{0.44}In_{0.56}As$ , of double-phonon-resonance design [13,14], was adopted, except that the Ga composition was increased by 2.5% in the wells in order to shift the net strain of the QCL design from the originally compressive strain value of  $-4.94(x10^{-4})$  to a net tensile strained value of 4.80  $(x10^{-4})$  relatively to the InP buffer's in-plane lattice constant. As discussed below, we find that within the scope of the growth conditions utilized in this study, studies on SL samples indicate that a net tensile strain is preferred. This active region design was chosen to avoid excessive individual-layer strain, while maintaining a relatively low net-tensile-strain value. The schematic diagram of the 1  $\mu m$  thick SL with InP capping layer, and the completed QCL structure grown on InP or GaAs, is shown in Fig. 1.

#### 3. Material characterizations

The surface morphology/roughness and structural properties from atomic force microscopy (AFM) and high-resolution X-ray diffraction (HR-XRD) measurements were used to identify an optimal net-strain value for the SL growth. Fig. 2(a) to (e) shows the surface morphology of the InP cap layer on top of the 250 repetitions of 2/2 nm InGaAs/ AlInAs superlattices for five samples (A to E) with different net strain target presented in Table 1. The upper left image, sample A (Fig. 2 (a)), shows high peak-to-valley amplitude likely generated from a 3D growth mode due to an excessive amount of net compressive strain. As the net strain is increased towards the tensile side, different surface morphology was observed, from large pinholes (Fig. 2(b)) to grains (Fig. 2(c)), smooth surface with less pinholes (Fig. 2(d)), to stepped surface with micro-cracking (Fig. 2(e)) from sample B to sample E. Only sample D has a shiny mirror-like appearance; others are hazy in appearance to the eye. The surface morphology of InP capping layer should roughly reflect the morphology of superlattice underneath, given the InP thickness is relatively thin, and the SLs do not exhibit significant strain relaxation, as confirmed from asymmetric reciprocal space mapping (RSM) XRD measurements.

HR-XRD  $\omega$ -2 $\theta$  scans along (004) InP diffraction are shown in Fig. 3. Narrow -1st satellite peak width (196 vs. 278 arcsecond) was observed for sample D compared to sample C and even the higher order satellite peak at large angle (around -18000 arcsecond) position could be seen on the compressive strain side, although significantly wider than the simulation. The simulation also fits well for sample D in terms of the expected target composition and layer thickness. Another observation is from sample A in that the zero-order superlattice peak is coincident with the InP peak, due to the out-of-plane lattice constant of sample A being matched to the InP buffer layer. Also, for samples B and E, we can observe that partial relaxation is evident for those net SL strain values, given the fact that all superlattice peaks are relatively broad and weak in intensity, and that shoulder peaks are observed just to the right of the superlattice peaks near -9000 and -13000 arcseconds. As little strain relaxation was observed for the SL samples from reciprocal space

Table 1

V/III ratios and growth rates for strained InGaAs and AlInAs superlattices grown on an InP buffer layer with designed net-strain target. The InP buffer's in-plane lattice constant is taken to be 0.5867 nm. The negative sign corresponds to compressive strain.

Sample	A	В	С	D	E
250x 2/2nm SLs	In <sub>0.75</sub> Ga <sub>0.25</sub> As Al <sub>0.70</sub> In <sub>0.30</sub> As	In <sub>0.72</sub> Ga <sub>0.28</sub> As Al <sub>0.685</sub> In <sub>0.315</sub> As	In <sub>0.73</sub> Ga <sub>0.27</sub> As Al <sub>0.70</sub> In <sub>0.30</sub> As	In <sub>0.712</sub> Ga <sub>0.288</sub> As Al <sub>0.685</sub> In <sub>0.315</sub> As	In <sub>0.71</sub> Ga <sub>0.29</sub> As Al <sub>0.685</sub> In <sub>0.315</sub> As
Individual layer strain $(\times 10^{-2})$	-3.07/2.97	-2.66/2.77	-3.00/2.97	-2.55/2.77	-2.52/2.77
V/III ratio	217.9/256.1	243.0/250.3	234.7/256.1	249.7/250.3	251.3/250.3
Growth rate (nm/s)	0.394/0.331	0.350/0.339	0.363/0.331	0.340/0.339	0.338/0.339
Target net strain $(\times 10^{-4})$	-2.55	2.72	4.35	5.48	6.17

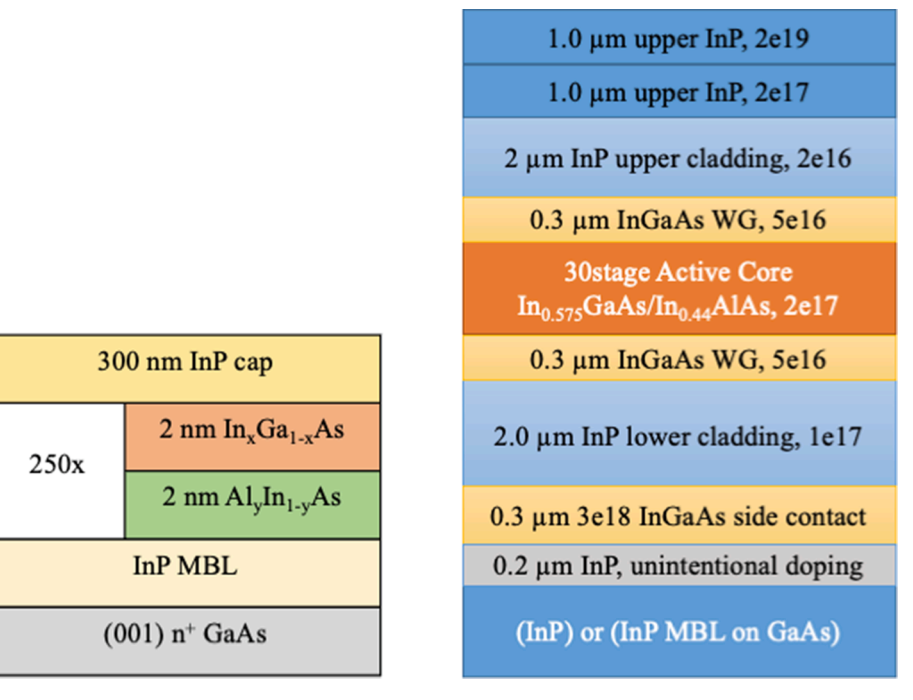


Fig. 1. (left). Diagram of 250 repetitions of 2/2 nm InGaAs/AlInAs superlattices grown on InP metamorphic buffer layers on GaAs with 300 nm capping; (right). Schematic representation of the completed 30-stage, strain-balanced QCL laser structure on n-doped InP or InP MBL on n-doped GaAs.

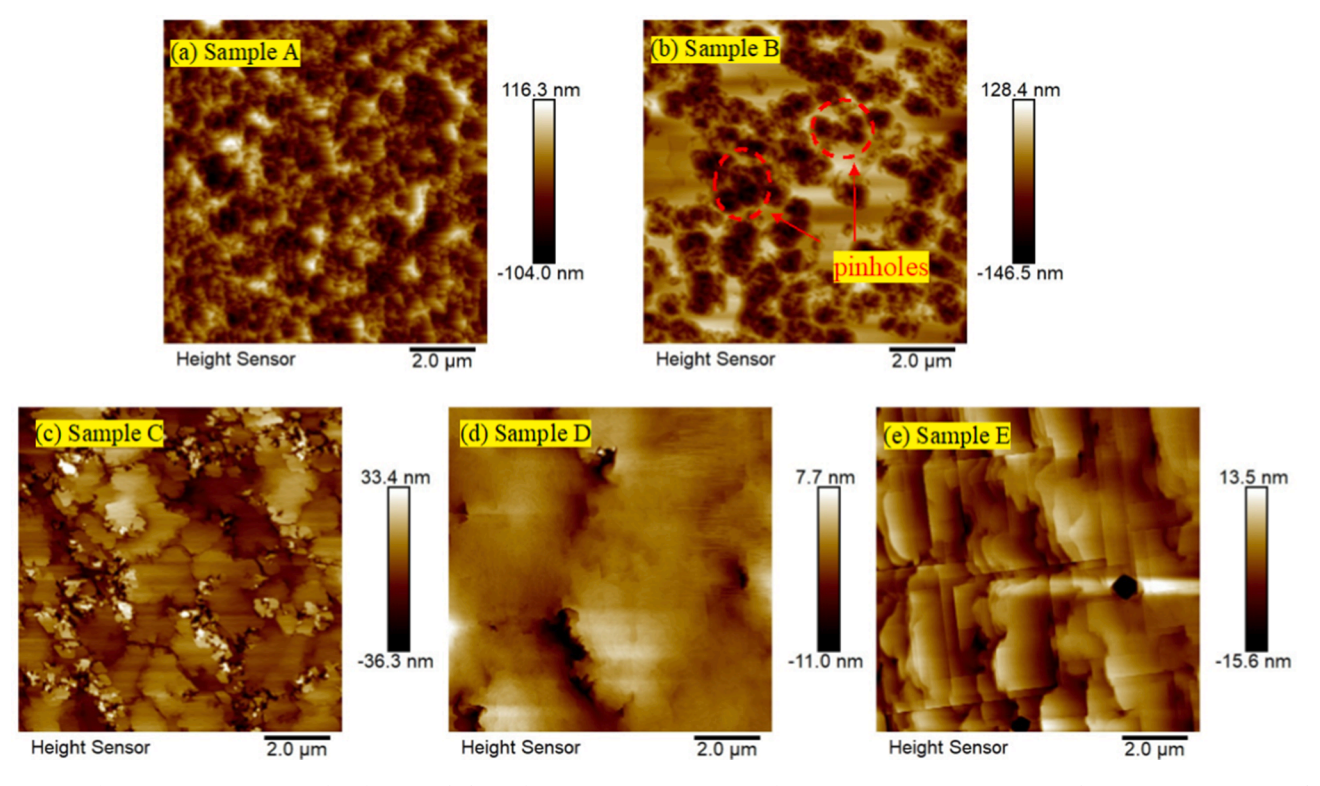


Fig. 2. Atomic force microscopy images of surface morphology after growing 250-repitation of 2 nm ( $\Delta a/a \sim -1.4\%$ ) InGaAs and 2 nm ( $\Delta a/a \sim +1.4\%$ ) AlInAs superlattices with different net strain targets, capped with a 300 nm InP layer. Sample A to sample E shown in Table 1 was labeled as (a) to (e), respectively.

mappings (RSM) XRD measurements, the -2nd and +2nd additional satellite peaks, observed in sample B and E, may originated from layers with different periodicity but same net-strain. The dual peaks may be explained by the discrepancy in arrangements of group-III atoms relative to group-V atoms, which is caused by the atomic ordering in the presence of large dislocation density at interfaces and excessive local strain

[15]. Thus, a distortion in lattice spacing would give the rise of the secondary peaks while the net strain was maintained as same, in turn, no peak splitting is observed for the 0th satellite peak. However, further investigations are required to confirm the underlying growth mechanism.

In theory, an infinite stack of alternating tensile and compressive

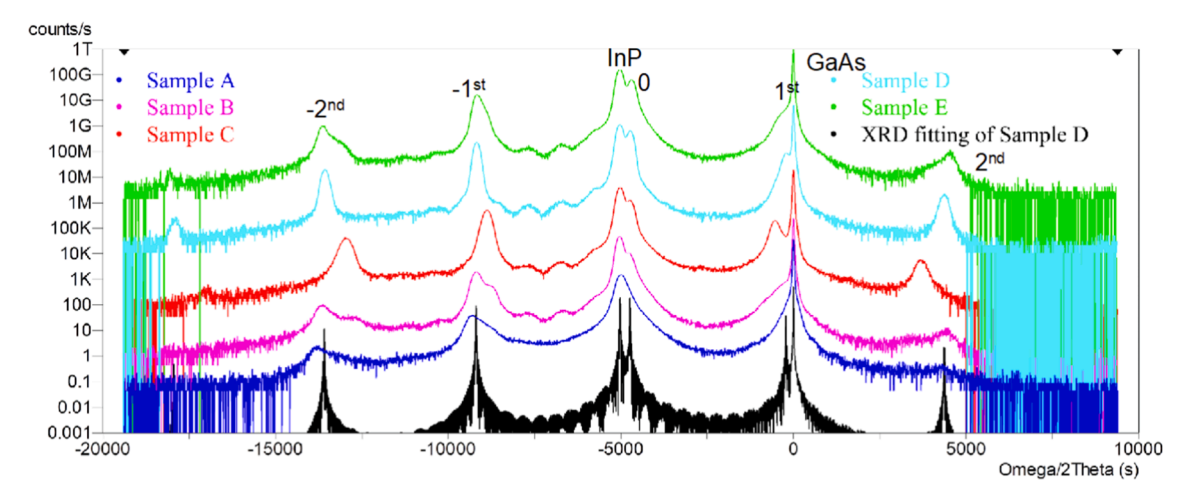


Fig. 3. HR-XRD  $\omega$ -2 $\theta$  measurements of 250 repetitions of 2/2nm InGaAs/AlInAs grown on an InP buffer. The dynamic XRD simulation was fitted for sample D with a result of 2.08/2.08 nm In<sub>0.712</sub>Ga<sub>0.288</sub>As/Al<sub>0.685</sub>In<sub>0.315</sub>As and a 97.4% relaxed InP cap. The intensity is offset to see each sample's satellite peaks.

layers could be designed and grown as long as there is zero net strain relative to the native substrate, and for such low net strain in this study, on the order of 10<sup>-4</sup> range, the critical thickness for the onset of strain relaxation of the SL is expected, based on the Matthews-Blakeslee model [16,17], to be greater than 1000 nm on a native (001) InP substrate. The "effective" critical thickness of the SL epilayers could be significantly reduced by CuPt-type atomic ordering effect, which has been intensively studied in photovoltaics employing a strained-layer InGaAs/GaAsP MQW system [18]. However, when considering the large density of dislocations and misfits present in the InP buffer [8], dislocations gliding through ordered planes (typically 60° on {111} planes for III-Vs) or glide plane switching generated by a new dislocation formation led to the creation of anti-phase boundary (APB), in order to minimize the strain energy, while group-III sublattice ordering in III-V epilayers could be altered to distort bonding [19-21]. Also, the CuPt ordering process is strongly dependent on the growth conditions as well as the use of surfactants [21]. By contrast to MBE growth, the MOVPE growth process promotes ordering, since hydrogen atoms assist in the surface reconstruction by providing additional electrons so as to satisfy the electron counting for group-V neighboring atom pairs [21,22]. We previously observed that dislocations prohibited the planar-layer growth of similar strained QCL structures grown on Si, for which only 5 stages of SL active region could be successfully grown, and large pits were observed to disrupt the consecutive superlattice layers in the vicinity of the threading dislocations by high-resolution transmission microscope (HR-TEM) [23]. The low mobility of Al atoms may be a contributing factor for non-step-flow growth mode which leads to material degradation for thick SL films.

Through careful SL strain balancing by taking into account the InP buffer layer in-plane lattice constant, tight net-strain control was achieved allowing for the growth of relatively higher strained InGaAs/AlI-nAs SL materials, which is essential for realizing mid-IR light sources on mismatched substrates.

Our previous attempts in growing strain-balanced QCLs on mismatched substrate, revealed a rapid intensity reduction of the *in-situ* reflectance measurement after growing about 10 stages of the active region [24]. In the current work, by optimizing the net strain of the active region, we observe that the *in-situ* reflectance intensity reduction is minimal during the entire strained 30-stage active region growth, similar to that observed for the growth of the lattice-matched QCL [8]. In addition, sharp and clear reflection interference fringes were observed and maintained for the entire growth.

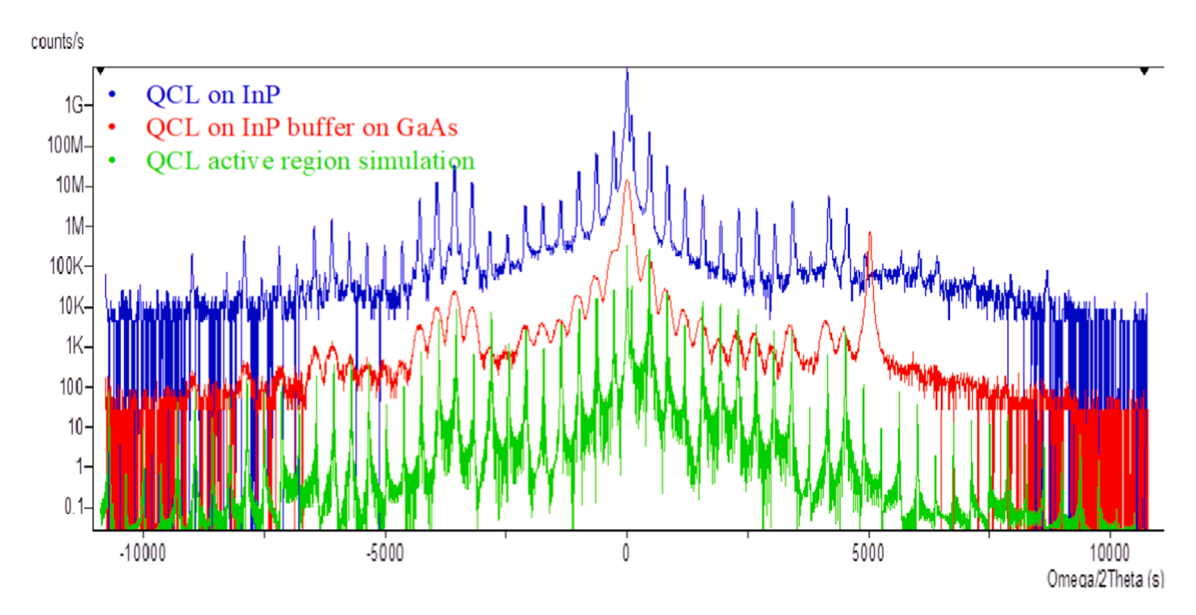


Fig. 4. Comparison of HR-XRD  $\omega$ -2 $\theta$  measurements for completed QCL structure with 30-stage, strain-balanced In Ga<sub>0.425</sub>As/Al<sub>0.56</sub>In<sub>0.44</sub>As active region grown on InP, and on InP buffer on GaAs with simulation. The intensity is offset to see the satellite peaks.

HR-XRD measurements along the (004) direction for the completed strain-balanced QCL structures grown on InP, and on InP buffer on GaAs are shown in Fig. 4. Although satellite peak broadening is observed for the QCL on GaAs compared with the QCL on InP, superlattice peaks are clearly defined, in contrast to the observation of weak intensity satellite peaks for MBE-grown strained QCLs on GaAs [6] and Si [7]. The fullwidth at half-maximum value (FWHM) for the QCL on GaAs was  $\sim$ 119 arcsecond for the InP main peak and increased to  $\sim$ 171 arcsecond for the highest satellite peak, while the FWHM value for the QCL on InP was  $\sim \! 31$  arcsecond for the InP peak and was reduced to  $\sim \! 29$  arcsecond for the highest satellite peak. Relatively high dislocation density [25] and possibly rougher interfaces of active-region superlattice may be further contributing to satellite peak broadening. Further studies are required to understand the interfacial structure of strained QCLs on a mismatched substrate using atom probe microscopy (APT), similar to the interface roughness analysis that we have done for strained QCL on native InP previously [26].

#### 4. Device performance characterization

The laser fabrication process was identical that used previously for realizing deep-etched 8.5 µm-emitting lattice-matched OCLs with episide current injection [8]. As shown in Fig. 5(a), the threshold-current density of the device on InP is about 25% higher than that for the device on GaAs, 2.16 vs. 1.61 kA/cm<sup>2</sup>. Higher maximum output power is observed on InP, 3.79 vs. 2.65 W respectively. In addition, the dynamic range for the devices grown on InP is also larger than for those grown on GaAs. This trend was also observed in a prior study on MOVPE-grown 8.5 µm-emitting lattice-matched QCL on GaAs [8]. By contrast, data for MBE-grown ternary InP-based InGaAs/AlInAs QCLs on mismatched substrates show significantly higher threshold-current densities than on native substrate [4-7]. The series resistance for the device grown on GaAs is higher than for that grown on InP, 1.75 vs. 1.24 Ohms, although the peak voltages are similar, indicating the structural properties for growths on GaAs and InP were similar, also evident from HR-XRD measurements described above. The slope efficiency and wall-plug efficiency values are 1.35 W/A and 6.0% for devices on GaAs and are 1.23 W/A and 5.5% for devices on InP, respectively. The high density of defects present on the MBL may result in reduced silicon-dopant incorporation or in reduced electron concentration in the QCL injector region, leading to the observed performance trends. Based on temperaturedependence measurements, from 20 to 60 °C, the extracted

characteristic temperatures,  $T_0$  and  $T_1$ , are 188 K and 324 K for devices grown on GaAs, and 159 K and 319 K for devices grown on InP. Fig. 5(b) and 5(c) show the lasing spectrum for devices operating just above the threshold current, at room temperature. The emission wavelength is centered around 5.71  $\mu$ m for devices grown on both InP and GaAs. Note that the performance achieved here is comparable to that reported previously for a similar QCL active-region design grown on InP substrate [9]. The wavelength shift from 5.29  $\mu$ m [9] to 5.71  $\mu$ m is expected since for the current work the Ga composition was increased by 2.5% in the quantum wells.

#### 5. Conclusion

Through a systematic study on the impact of net strain on the growth of 1 µm-thick strained superlattices on buffer layers with a high density of dislocations, we have found, a small mismatch between the in-plane lattice constant of the InP buffer and native InP can lead to undesirable surface morphology and structural degradation of the SL. The sensitivity observed for the overall net strain stems from the critical thickness for strained-layer materials being significantly reduced in the presence of defects and a net tensile strain condition was established which allows for the growth of thick SLs and QCL active regions, although this strain value may be dependent on specific MOVPE growth conditions. Based on the above findings, we adjusted the compositions to more effectively balance the net strain to allow for the growth of the QCL active region and, in turn, we demonstrated the first InGaAs/ AlInAs/InP-based strained-balanced QCL grown by MOVPE on GaAs. The QCL devices emit at 5.7 µm wavelength and show comparable laser performance to their counterparts grown on native InP. This work helps elucidate the growth-condition optimizations required for realizing high-strain thick superlattices via MOVPE on lattice mismatched substrates, and subsequently for the realization of high-performance QCLs on non-native substrates.

# CRediT authorship contribution statement

Shining Xu: Conceptualization, Methodology, Writing – original draft. Shuqi Zhang: Investigation. Huilong Gao: Investigation. Jeremy Kirch: Investigation, Writing – review & editing. Dan Botez: Supervision, Writing – review & editing. Luke Mawst: Conceptualization, Supervision, Writing – review & editing.

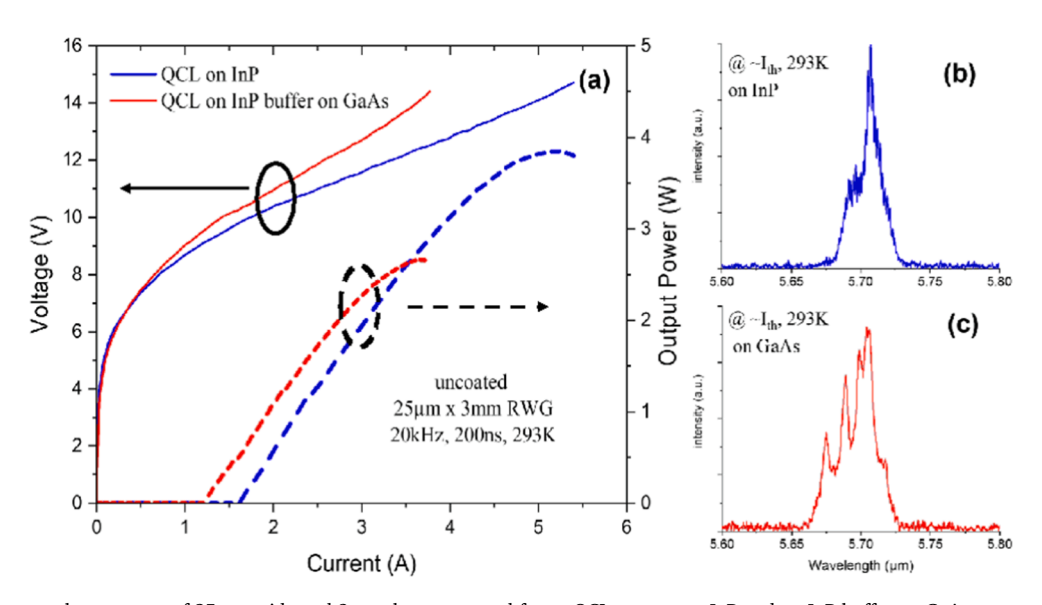


Fig. 5. (a) Light-current–voltage curves of 25 μm wide and 3 mm long uncoated-facets QCLs grown on InP and on InP buffer on GaAs measured under pulse-mode operation at room temperature. Just above threshold lasing spectra for devices: (b) on InP, and (c) on InP buffer on GaAs.

#### **Declaration of Competing Interest**

The authors declare the following financial interests/personal relationships which may be considered as potential competing interests: Luke Mawst reports a relationship with Intraband LLC that includes: consulting or advisory.

#### Data availability

Data will be made available on request.

#### Acknowledgement

This work was primarily supported by National Science Foundation (ECCS 1806285). The authors gratefully acknowledge use of facilities and instrumentation at the UW-Madison Wisconsin Centers for Nanoscale Technology, partially supported by the NSF through the University of Wisconsin Materials Research Science and Engineering Center (DMR-1720415).

#### References

- L.J. Mawst, D. Botez, High-power mid-infrared (λ~3-6 μm) quantum cascade lasers, IEEE Photonics J. 14 (2022) 1–25, https://doi.org/10.1109/ JPHOT.2021.3132261.
- [2] D. Botez, C.-C. Chang, L.J. Mawst, Temperature sensitivity of the electro-optical characteristics for mid-infrared (λ = 3–16 μm)-emitting quantum cascade lasers, J. Phys. D: Appl. Phys. 49 (2016), 043001. https://iopscience.iop.org/article/10 .1088/0022-3727/49/4/043001.
- [3] Y. Bai, N. Bandyopadhyay, S. Tsao, S. Slivken, M. Razeghi, Room temperature quantum cascade lasers with 27% wall plug efficiency, Appl. Phys. Lett. 98 (2011), 181102. https://doi.org/10.1063/1.3586773.
- [4] R. Go, H. Krysiak, M. Fetters, P. Figueiredo, M. Suttinger, J. Leshin, X.M. Fang, J. M. Fastenau, D. Lubyshev, A.W.K. Liu, A. Eisenbach, M.J. Furlong, A. Lyakh, Room temperature operation of quantum cascade lasers monolithically integrated onto a lattice-mismatched substrate, Appl. Phys. Lett. 112 (2018), 031103, https://doi.org/10.1063/1.5012503.
- [5] R. Go, H. Krysiak, M. Fetters, P. Figueiredo, M. Suttinger, X.M. Fang, A. Eisenbach, J.M. Fastenau, D. Lubyshev, A.W.K. Liu, N.G. Huy, A.O. Morgan, S.A. Edwards, M. J. Furlong, A. Lyakh, InP-based quantum cascade lasers monolithically integrated onto silicon, Opt. Exp. 26 (2018) 22389, https://doi.org/10.1364/OE.26.022389.
- [6] S. Slivken, M. Razeghi, High power mid-infrared quantum cascade lasers grown on GaAs, Photonics 9 (2022) 231, https://doi.org/10.3390/photonics9040231.
- [7] S. Slivken, N. Shrestha, M. Razeghi, High power mid-infrared quantum cascade lasers grown on Si, Photonics 9 (2022) 626, https://doi.org/10.3390/ photonics9090626.
- [8] S. Xu, S. Zhang, J.D. Kirch, S. Suri, N. Pokharel, H. Gao, H. Kim, P. Dhingra, M. L. Lee, D. Botez, L.J. Mawst,  $\sim$ 8.5  $\mu$  m-emitting InP-based quantum cascade lasers grown on GaAs by metal-organic chemical vapor deposition, Appl. Phys. Lett. 121 (2022), 171103, https://doi.org/10.1063/5.0122272.

- [9] E. Kasper, H. Kibbel, H. Jorke, H. Brugger, E. Friess, G. Abstreiter, symmetrically strained Si/Ge superlattices on Si substrates, Phys. Rev. B 38 (1988) 3599–3601, https://doi.org/10.1103/PhysRevB.38.3599.
- [10] K. Nakajima, Calculation of stresses in GaAs/Si strained heterostructures, J. Cryst. Growth 121 (1992) 278–296, https://doi.org/10.1016/0022-0248(92)90138-9.
- [11] B.R. Bennett, J.A. del Alamo, Mismatched InGaAs/InP and InAlAs/InP heterostructures with high crystalline quality, J. Appl. Phys. 73 (1993) 3195–3202, https://doi.org/10.1063/1.352963.
- [12] N.J. Ekins-Daukes, K. Kawaguchi, J. Zhang, Strain-balanced criteria for multiple quantum well structures and its signature in X-ray rocking curves, Cryst. Growth Des. 2 (2002) 287–292, https://doi.org/10.1021/cg025502y.
- [13] L. Diehl, D. Bour, S. Corzine, J. Zhu, G. Höfler, M. Lončar, M. Troccoli, F. Capasso, High-temperature continuous wave operation of strain-balanced quantum cascade lasers grown by metal organic vapor-phase epitaxy, Appl. Phys. Lett. 89 (2006), 081101, https://doi.org/10.1063/1.2337284.
- [14] D. Hofstetter, M. Beck, T. Aellen, J. Faist, High-temperature operation of distributed feedback quantum-cascade lasers at 5.3 μm, Appl. Phys. Lett. 78 (2001) 396–398, https://doi.org/10.1063/1.1340865.
- [15] G.B. Stringfellow, G.S. Chen, Atomic ordering in III/V semiconductor alloys, J. Vac. Sci. Technol. B. 9 (1991) 2182, https://doi.org/10.1116/1.585761.
- [16] J. Matthews, Defects in epitaxial multilayers I. Misfit dislocations, Journal of Crystal Growth. 27 (1974) 118–125, https://doi.org/10.1016/0022-0248(74) 90424-2.
- [17] S.M. Hu, Misfit dislocations and critical thickness of heteroepitaxy, J. Appl. Phys. 69 (1991) 7901–7903, https://doi.org/10.1063/1.347476.
- [18] H. Fujii, Y. Wang, K. Watanabe, M. Sugiyama, Y. Nakano, Suppressed lattice relaxation during InGaAs/GaAsP MQW growth with InGaAs and GaAs ultra-thin interlayers, J. Cryst. Growth 352 (2012) 239–244, https://doi.org/10.1016/j. icrysgro.2011.11.036.
- [19] B.A. Philips, A.G. Norman, T.Y. Seong, S. Mahajan, G.R. Booker, M. Skowronski, J. P. Harbison, V.G. Keramidas, Mechanism for CuPt-type ordering in mixed III–V epitaxial layers, J. Cryst. Growth 140 (1994) 249–263, https://doi.org/10.1016/0022-0248(94)90297-6.
- [20] W.E. McMahon, J. Kang, R.M. France, A.G. Norman, D.J. Friedman, S.-H. Wei, Ordering-enhanced dislocation glide in III-V alloys, J. Appl. Phys. 114 (2013), 203506. https://doi.org/10.1063/1.4833244.
- [21] R.M. France, W.E. McMahon, H.L. Guthrey, Critical thickness of atomically ordered III-V alloys, Appl. Phys. Lett. 107 (2015), 151903, https://doi.org/10.1063/ 1.4933092.
- [22] I.G. Batyrev, W.E. McMahon, S.B. Zhang, J.M. Olson, S.-H. Wei, Step structures on III-V phosphide (0 0 1) surfaces: how do steps and Sb affect CuPt ordering of G a I n P 2 ? Phys. Rev. Lett. 94 (2005), 096101 https://doi.org/10.1103/ PhysRevLett.94.096101.
- [23] A. Rajeev, B. Shi, Q. Li, J.D. Kirch, M. Cheng, A. Tan, H. Kim, K. Oresick, C. Sigler, K.M. Lau, T.F. Kuech, L.J. Mawst, III-V superlattices on InP/Si metamorphic buffer layers for λ ≈4.8 μm quantum cascade lasers, Phys. Status Solidi A. (2018) 1800493, https://doi.org/10.1002/pssa.201800493.
- [24] S. Xu, H. Kim, B. Knipfer, J.D. Kirch, D. Botez, and L.J. Mawst, InGaAs/AlInAs/InP Quantum Cascade Laser Grown on GaAs with Strained QW-based Dislocation Filters ACCGE-22//OMVPE-20 Workshop, 2021.
- [25] J.E. Ayers, The measurement of threading dislocation densities in semiconductor crystals by X-ray diffraction, J. Cryst. Growth 135 (1994) 71–77, https://doi.org/ 10.1016/0022-0248(94)90727-7.
- [26] B. Knipfer, S. Xu, J.D. Kirch, D. Botez, L.J. Mawst, Analysis of interface roughness in strained InGaAs/AlInAs quantum cascade laser structures ( $\lambda \sim 4.6~\mu m$ ) by atom probe tomography, J. Cryst. Growth 583 (2022), 126531, https://doi.org/10.1016/j.jcrysgro.2022.126531.